

# Triazine Based Bipolar Host Materials for Blue Phosphorescent OLEDs

Daniel Wagner,<sup>†</sup> Sebastian T. Hoffmann,<sup>‡</sup> Ute Heinemeyer,<sup>§</sup> Ingo Münster,<sup>§</sup> Anna Köhler,<sup>‡</sup> and Peter Strohriegel<sup>†,\*</sup>

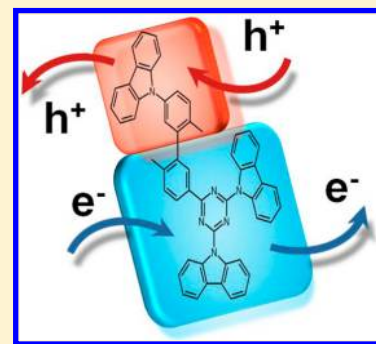
<sup>†</sup>Makromolekulare Chemie I and Bayreuther Institut für Makromolekülforschung, University of Bayreuth, 95440 Bayreuth, Germany

<sup>‡</sup>Experimentalphysik II, University of Bayreuth, 95440 Bayreuth, Germany

<sup>§</sup>BASF SE, 67056 Ludwigshafen, Germany

**ABSTRACT:** Two novel bipolar host materials BPTRZ and MBPTRZ were synthesized, in which the hole transporting carbazole is separated from the electron transporting triazine moiety by a fully aromatic, but nonconjugated meta-linked biphenyl unit. The additional twist at the biphenyl in MBPTRZ, which is achieved by methyl-substitution in 2- and 2'-position of the biphenyl leads to a higher triplet energy of 2.81 eV compared to 2.70 eV for BPTRZ. Both materials possess high thermal stabilities and good glass forming properties. An organic light emitting diode with MBPTRZ as host for the blue phosphorescence emitter FIrpic shows a maximum luminance of 30600 cd/m<sup>2</sup> and a maximum external quantum efficiency of 7.0%.

**KEYWORDS:** host material, bipolar, triazine, carbazole, phosphorescence, blue OLED



## INTRODUCTION

The discovery of phosphorescent emitters was one of the major breakthroughs toward efficient OLEDs. According to spin statistics, 75% triplet excitons and 25% singlet excitons are formed by the recombination of an electron and a hole. By harvesting both singlet and triplet excitons through intersystem crossing (ISC), phosphorescent organic light emitting diodes (PhOLEDs) approach 100% internal quantum efficiency.<sup>1,2</sup> In a PhOLED, the phosphorescent emitter is usually embedded in a suitable host to avoid self-quenching and triplet-triplet-annihilation. For an efficient energy transfer, it is essential that the triplet energy of the host is higher compared to the emitter to prevent reverse energy transfer from the emitter back to the host and to confine triplet excitons effectively on the emitter molecules.<sup>3,4</sup> Effective host-guest systems have been commercialized for green and red emitters, whereas blue phosphors and suitable matrix materials are still a challenge. The best known blue emitter is the light blue bis[(4',6'-difluorophenyl)pyridinato-N,C<sup>2'</sup>]iridium(III) picolinate (FIrpic) with a triplet energy of 2.65 eV (470 nm).<sup>4</sup> Other blue phosphors with a more saturated blue emission are iridium(III) bis(4',6'-difluorophenylpyridinato)tetrakis(1-pyrazolyl)borate (FIr<sub>6</sub>) and *mer*-tris(*N*-dibenzofuranyl-*N'*-methylimidazole)iridium(III) (Ir(dbfmi)) showing triplet levels of 2.72 eV (458 nm)<sup>5</sup> and 2.79 eV (445 nm).<sup>6</sup>

The confinement of the conjugated system is the key to host materials with high triplet energies. A widely used host material for green and red emitters is 4,4'-bis(9-carbazolyl)-biphenyl (CBP) with a triplet level of 2.56 eV.<sup>3</sup> By replacing the central biphenyl group in CBP by a single, meta-linked benzene unit,

*N,N'*-dicarbazolyl-3,5-benzene (mCP) with a high triplet energy of 2.90 eV has been reported as host material for saturated blue OLEDs.<sup>4,7</sup> The introduction of torsion in the biphenyl unit of the host material 4,4'-bis(9-carbazolyl-2,2'-dimethylbiphenyl) (CDBP) caused by steric hindrance of two methyl substituents in 2- and 2'-position leads to a triplet energy of 2.79 eV.<sup>8,9</sup> By tuning the linking between the carbazole and the central biphenyl unit from the para to the meta position, the triplet energy in 3,3'-bis(carbazolyl)biphenyl (m-CBP)<sup>10,11</sup> is enlarged to 2.98 eV.<sup>11</sup>

To achieve efficient OLEDs a balanced charge carrier transport and a broad recombination zone are required. By the design of bipolar host materials, this task can be accomplished.<sup>12</sup> In bipolar host materials, holes and electrons are transported through different parts of the molecule. The hole transport in many cases occurs through carbazole units due to sufficiently high triplet energy and good hole transporting properties,<sup>13,14</sup> whereas electron transport is often realized by the use of electron accepting *N*-heterocycles such as triazines<sup>15</sup> or oxadiazoles.<sup>16</sup> In recent years, a number of bipolar host materials such as 2,6-bis(3-(carbazol-9-yl)phenyl)pyridine (26DCzPPy)<sup>17</sup> and bis-4-(*N*-carbazolyl)phenyl)phenylphosphine oxide (BCPO)<sup>18</sup> have been described. The literature on bipolar host materials has been summarized by Chaskar et al.<sup>19</sup>

1,3,5-triazine derivatives such as 3-(4,6-diphenyl-1,3,5-triazine-2-yl)-9-phenyl-9H-carbazole (DPTPCz),<sup>20</sup> 2-(3-(*N,N*-bis(4-(1,1-dimethylethyl)phenyl)-amino)phenyl)-phenyl)-4,6-diphenyl-1,3,5-triazine (tBu-TPA-m-TRZ),<sup>21</sup> 9-(4,6-diphenyl-1,3,5-triazine-2-yl)-9'-phenyl-3,3'-bicarbazole (CzT),<sup>22</sup> and 2-

**Published:** August 13, 2013

(4-(3,6-dimethylcarbazol-9-yl)-phenoxy)-bis-4,6-biscarbazolyl-1,3,5-triazine (PCTrz)<sup>23</sup> have been reported as bipolar host materials owing to the high triplet energies and the excellent electron transport ability of the triazine moiety.

In a previous paper, we have presented the bipolar matrix material PCTrz with a hole transporting carbazole and an electron transporting triazine moiety.<sup>23</sup> By using the concepts of twisted<sup>24</sup> or meta-linked<sup>11</sup> biphenyls to break the conjugation, we have achieved CBP-like materials with large triplet energies. Here, we present a combination of both concepts. In the two novel bipolar matrix materials BPTRZ and MBPTRZ, a hole transporting carbazole and an electron transporting triazine moiety are connected by a fully aromatic but nonconjugated biphenyl bridging group.

## ■ EXPERIMENTAL SECTION

**Materials.** All chemicals and reagents were used as received from commercial sources without further purification. The solvents for reactions and purification were distilled before use.

**2,4-Bis(carbazol-9-yl)-6-chloro-1,3,5-triazine (1).** Compound 1 was synthesized according to a procedure reported by Rothmann et al.<sup>25</sup> Yield: 70%.

**3,3'-Dibromobiphenyl (2).** 3-Bromophenylboronic acid (5.0 g, 24.9 mmol) was dissolved in methanol (65 mL). After addition of copper(I) chloride (0.05 g, 0.51 mmol), the mixture was stirred at room temperature for 4 h in air. The reaction mixture was filtered and washed with ethyl acetate. The solvent was evaporated and the crude product was purified by column chromatography on silica gel with hexane as eluent to afford 2.32 g (7.4 mmol, 60%) of 2 as white solid. <sup>1</sup>H NMR (300 MHz, CDCl<sub>3</sub>),  $\delta$  (ppm): 7.70 (t, 2H), 7.52–7.45 (m, 4H), 7.31 (t, 2H). <sup>13</sup>C NMR (75 MHz, CDCl<sub>3</sub>),  $\delta$  (ppm): 141.9, 130.9, 130.5, 130.3, 125.9, 132.1. EI-MS *m/z*: 312 (100, M<sup>+</sup>), 152 (100), 76 (51).

**3,3'-Diiodo-6,6'-dimethylbiphenyl (3).** Compound 3 was synthesized according to the procedure reported by Schrögel et al.<sup>11</sup> Yield: 32%.

**General Procedure for Ullmann-type Reaction.** The 3,3'-dihalogenobiphenyls 2 or 3 (9.2 mmol), carbazole (1.54 g, 9.2 mmol), copper iodide (0.18 g, 0.9 mmol), trans-1,2-diaminocyclohexane (0.11 g, 0.9 mmol), and potassium phosphate (4.11 g, 19.4 mmol) were dissolved in dioxane (60 mL) under argon atmosphere. The mixture was refluxed for 20 h. After cooling to room temperature, the mixture was diluted with THF. The copper catalyst and inorganic salts were removed by filtration over neutral aluminum oxide. The solvent was evaporated and the residue was purified by column chromatography on silica gel with hexane/toluene (4:1) as eluent to yield 4 and 5 as light yellow solids.

**3-(Carbazol-9-yl)-3'-bromobiphenyl (4).** Yield: 47%. <sup>1</sup>H NMR (300 MHz, CDCl<sub>3</sub>),  $\delta$  (ppm): 8.17 (dt, 2H), 7.78 (dt, 2H), 7.73–7.63 (m, 2H), 7.61–7.39 (m, 7H), 7.37–7.27 (m, 3H). <sup>13</sup>C NMR (75 MHz, CDCl<sub>3</sub>),  $\delta$  (ppm): 142.3, 141.8, 140.9, 138.5, 130.9, 130.6, 130.4, 126.6, 126.3, 126.0, 125.9, 125.8, 123.6, 123.2, 120.5, 120.2, 109.8. EI-MS *m/z*: 398 (100, M<sup>+</sup>), 317 (24), 159 (21).

**3-(Carbazol-9-yl)-6,6-dimethyl-3'-iodobiphenyl (5).** Yield: 48%. <sup>1</sup>H NMR (300 MHz, CDCl<sub>3</sub>),  $\delta$  (ppm): 8.14 (d, 2H), 7.62–7.54 (m, 2H), 7.48 (s, 2H), 7.42 (d, 4H), 7.31–7.15 (m, 3H), 7.04 (d, 1H), 2.18 (s, 3H), 2.12 (s, 3H). <sup>13</sup>C NMR (75 MHz, CDCl<sub>3</sub>),  $\delta$  (ppm): 142.9, 141.7, 141.0, 137.8, 136.7, 135.6, 135.4, 135.3, 132.1, 131.6, 127.6, 126.3, 126.0, 123.4, 120.4, 120.0, 109.8, 90.6, 19.7. EI-MS *m/z*: 473 (100, M<sup>+</sup>), 165 (35), 91 (20).

**General Procedure for Miyaura-Borylation Reaction.** The 3-(carbazol-9-yl)-3'-halogenobiphenyls 4 or 5 (3.8 mmol), bis(pinacolato)diboron (1.05 g, 4.1 mmol), PdCl<sub>2</sub>(dppf) (0.09 g, 0.1 mmol) and anhydrous potassium acetate (1.11 g, 11.3 mmol) were dissolved in dry DMSO (50 mL) under argon atmosphere. The mixture was stirred at 80 °C for 3 h. After cooling to room temperature, the mixture was extracted with diethyl ether and washed several times with water. The organic phase was filtrated and the solvent was evaporated to yield 6 and 7 as light yellow solids.

**3-(Carbazol-9-yl)-3'-(4,4,5,5-tetramethyl-1,3,2-dioxaborolan)biphenyl (6).** Yield: 87%. <sup>1</sup>H NMR (300 MHz, CDCl<sub>3</sub>),  $\delta$  (ppm): 8.16 (d, 2H), 8.08 (s, 1H), 7.90–7.80 (m, 2H), 7.74 (dt, 2H), 7.66 (t, 1H), 7.53 (dt, 1H), 7.51–7.37 (m, 5H), 7.32–7.26 (m, 2H), 1.35 (s, 12H). <sup>13</sup>C NMR (75 MHz, CDCl<sub>3</sub>),  $\delta$  (ppm): 143.3, 141.0, 139.6, 138.2, 134.3, 133.7, 130.3, 130.1, 128.5, 126.5, 126.1, 126.0, 125.9, 123.5, 120.4, 120.0, 110.0, 84.1, 25.1, 25.0. EI-MS *m/z*: 445 (100, M<sup>+</sup>), 345 (36).

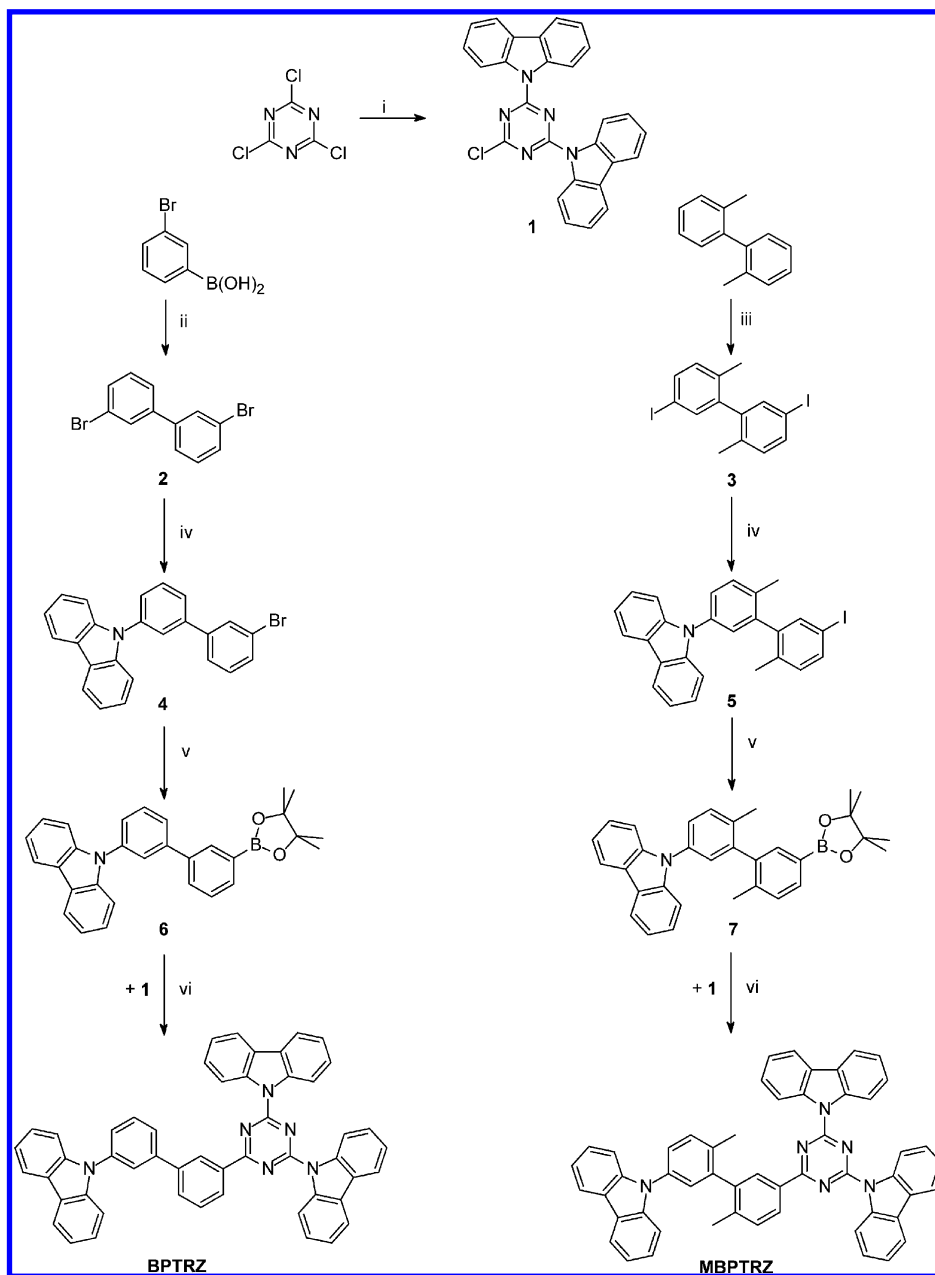
**3-(Carbazol-9-yl)-6,6'-dimethyl-3'-(4,4,5,5-tetramethyl-1,3,2-dioxaborolan)biphenyl (7).** Yield: 85%. <sup>1</sup>H NMR (300 MHz, CDCl<sub>3</sub>),  $\delta$  (ppm): 8.15 (d, 2H), 7.74 (d, 1H), 7.65 (s, 1H), 7.52–7.38 (m, 6H), 7.35–7.25 (m, 4H), 2.23 (s, 3H), 2.19 (s, 3H), 1.35 (s, 12H). <sup>13</sup>C NMR (75 MHz, CDCl<sub>3</sub>),  $\delta$  (ppm): 143.2, 141.1, 140.2, 139.3, 135.7, 135.6, 135.1, 134.1, 131.3, 129.6, 128.0, 126.0, 125.8, 123.4, 120.4, 119.8, 110.0, 83.9, 25.1, 25.0, 20.4, 19.8. EI-MS *m/z*: 473 (100, M<sup>+</sup>), 415 (22), 373 (88), 229 (23), 166 (52).

**General Procedure for Suzuki-Miyaura Cross-Coupling.** 2,4-Bis(carbazol-9-yl)-6-chloro-1,3,5-triazine 1 (0.71 g, 1.6 mmol) and 3-(carbazol-9-yl)-3'-(4,4,5,5-tetramethyl-1,3,2-dioxaborolan)biphenyl 6 or 7 (1.9 mmol) were dissolved in dioxane (65 mL) and toluene (22 mL). After the addition of potassium phosphate (0.57 g, 2.7 mmol) in 18 mL water, the mixture was degassed by three freeze–pump–thaw cycles and the flask was backfilled with argon. Pd<sub>2</sub>(dba)<sub>3</sub> (45 mg, 0.05 mmol) and PCy<sub>3</sub> (30 mg, 0.11 mmol) were added, and the mixture was degassed again by three freeze–thaw cycles and the flask backfilled with argon. The mixture was stirred at 90 °C for 20 h. After cooling to room temperature, the mixture was poured into water and then extracted with DCM. The combined organic phase was washed with water, filtered, and dried over sodium sulfate. The solvent was evaporated and the crude product was boiled in ethyl acetate and hot filtered to yield BPTRZ and MBPTRZ as white solids after cooling. The product was further purified by train sublimation.

**3-(Carbazol-9-yl)-3'-(4,6-(dicarbazol-9-yl)-1,3,5-triazin-2-yl)-1,1'-biphenyl (BPTRZ).** Yield: 52%. <sup>1</sup>H NMR (300 MHz, CDCl<sub>3</sub>),  $\delta$  (ppm): 9.11–9.00 (m, 5H), 8.73 (d, 1H), 8.20 (d, 2H), 8.12–8.03 (m, 4H), 7.98 (d, 2H), 7.90 (d, 1H), 7.82–7.71 (m, 2H), 7.66 (d, 1H), 7.52 (d, 2H), 7.43–7.27 (m, 12H). <sup>13</sup>C NMR (75 MHz, CDCl<sub>3</sub>),  $\delta$  (ppm): 172.6, 164.7, 142.3, 140.9, 140.6, 138.8, 136.8, 131.3, 130.6, 129.7, 128.4, 127.9, 127.0, 126.5, 126.1, 125.8, 123.4, 120.4, 120.0, 119.7, 117.5, 109.8. EI-MS *m/z*: 728 (100, M<sup>+</sup>), 344 (22), 166 (22).

**3-(Carbazol-9-yl)-6,6'-dimethyl-3'-(4,6-(dicarbazol-9-yl)-1,3,5-triazin-2-yl)-1,1'-biphenyl (MBPTRZ).** Yield: 92%. <sup>1</sup>H NMR (300 MHz, CDCl<sub>3</sub>),  $\delta$  (ppm): 9.03 (d, 4H), 8.62 (m, 2H), 8.16 (d, 2H), 8.09 (d, 4H), 7.62–7.28 (m, 18H), 2.37 (s, 3H), 2.35 (s, 3H). <sup>13</sup>C NMR (75 MHz, CDCl<sub>3</sub>),  $\delta$  (ppm): 172.8, 164.6, 142.4, 141.4, 141.1, 138.8, 135.4, 135.2, 133.8, 131.6, 130.9, 130.2, 128.3, 128.0, 126.9, 126.4, 126.3, 125.9, 123.3, 120.3, 119.8, 119.7, 117.4, 109.7, 20.4, 19.7. EI-MS *m/z*: 756 (100, M<sup>+</sup>), 378 (26), 166 (32).

**Characterization.** <sup>1</sup>H and <sup>13</sup>C NMR spectra were recorded with a Bruker AC-300 (300 MHz, 75 MHz) and CDCl<sub>3</sub> as solvent. All data were given as chemical shifts  $\delta$  (ppm) downfield from Si(CH<sub>3</sub>)<sub>4</sub>. MS spectra were received on a Finnigan Mat 8500, MAT 112 S Varian machine using EI-ionization. For differential scanning calorimetry measurements (DSC), a Perkin-Elmer Diamond DSC apparatus with heating and cooling rates of 10 K/min under nitrogen atmosphere was used. Thermogravimetric analysis (TGA) was performed on a Mettler Toledo TGA/SDTA851e machine at a heating rate of 10 K/min under a nitrogen atmosphere. Cyclic voltammetry measurements (CV) were performed with an EG&G Princeton Applied Research Potentiostat/Galvanostat Model 263 A. The measurements were carried out in absolute solvents measuring at a platinum working electrode vs a Ag/AgNO<sub>3</sub> reference electrode. Each measurement was calibrated against an internal standard (ferrocene/ferrocenium redox system). The target molecules were finally purified by sublimation at a Carbolite HZS 12/450 three zone tube furnace equipped with a Leybold PT 151/361 KIT turbomolecular pump. The purity of the target compounds was checked with a Waters size exclusion chromatography system (SEC) for oligomers (analytical columns, cross-linked polystyrene gel (Polymer Laboratories); length, 2 × 60 cm; width, 0.8 m; particle size, 5  $\mu$ m; pore size, 100 Å; eluent, THF (0.5 mL/min, 80 bar), polystyrene standard).

Scheme 1. Synthesis of BPTRZ and MBPTRZ<sup>a</sup>

<sup>a</sup>Reagents and conditions: (i) 2 equiv. carbazole, *n*-BuLi, THF, reflux, 6 h. (ii) CuCl, methanol, RT, 4 h. (iii) I<sub>2</sub>/HIO<sub>3</sub>, CHCl<sub>3</sub>, H<sub>2</sub>SO<sub>4</sub>, AcOH, H<sub>2</sub>O, 80 °C, 6.5 h. (iv) Carbazole, CuI, trans-1,2-diaminocyclohexane, K<sub>3</sub>PO<sub>4</sub>, dioxane, reflux, 20 h. (v) Bis(pinacolato)diboron, PdCl<sub>2</sub>(dppf), KOAc, DMSO, 80 °C, 3 h. (vi) Pd<sub>2</sub>dba<sub>3</sub>, PCy<sub>3</sub>, K<sub>3</sub>PO<sub>4</sub>, H<sub>2</sub>O, dioxane, toluene, 90 °C, 20 h.

**Spectroscopic Measurements.** All optical measurements were carried out on thin films. The films of about 150 nm thickness as determined by a Dektak profilometer were prepared by dissolving BPTRZ and MBPTRZ in toluene at a concentration of 20 mg/mL and casting films from this solution. Absorption spectra were measured with a Cary5000 spectrometer from Varian. Fluorescence spectra were obtained in a nitrogen-purged atmosphere from a JASCO FP-8600 luminescence spectrometer using excitation at 330 nm. The phosphorescence spectra were taken with the thin film samples mounted in a continuous flow helium cryostat. The temperature was controlled with an Oxford Intelligent temperature controller (ITC-502). Excitation was provided by a pulsed nitrogen laser (LTB MNL106PD) at 337.1 nm. The light emitted by the sample was dispersed and subsequently detected by a time gated intensified CCD camera (Andor iStar DH734-18F-9AM) with a delay time of 1  $\mu$ s and a

gate width of 10 ms. The measurements were carried out at an excitation density of about 10  $\mu$ J cm<sup>-2</sup> pulse<sup>-1</sup>.

**OLED Fabrication.** The ITO substrate (10 ohm/square) used as the anode is first cleaned with an acetone/isopropanol mixture in an ultrasonic bath. For eliminating any possible organic residues and for improving the hole injection, the substrate is thereafter exposed to ozone for 30 min. Then, Plexcore OC AJ20-1000 (commercially available from Plextronics Inc.) is spin-coated and dried to form a hole injection layer (~40 nm). Thereafter, the organic materials are applied by vapor deposition in ultrahigh vacuum (<10<sup>-6</sup> mbar).

**Computational Calculations.** Density Functional Theory (DFT) calculations were carried out using the B3LYP hybrid functional together with the basis set 6-311G\*.<sup>26,27</sup> The excited states were calculated by using Time-Dependent-DFT with the optimized ground-

state geometries. All DFT calculations were carried out with the Gaussian 09 program.

## RESULTS AND DISCUSSION

**Synthesis.** We have prepared the two novel matrix materials BPTRZ and MBPTRZ. In both materials, a triazine unit is

**Table 1. Thermal Properties of Matrix Materials BPTRZ and MBPTRZ<sup>a</sup>**

	$T_g$ (°C)	$T_m$ (°C)	$T_c$ (°C)	$T_d$ (°C)
BPTRZ	134	286, 290	228, 236 <sup>b</sup>	445
MBPTRZ	154	284 <sup>c</sup>	225 <sup>c</sup>	475

<sup>a</sup> $T_g$ : glass transition temperature;  $T_m$ : melting temperature;  $T_c$ : crystallization temperature;  $T_d$ : 1% weight loss in  $N_2$  atmosphere.  
<sup>b</sup>Observed only upon heating. <sup>c</sup>Observed only in the first heating scan.

connected to a carbazole by a fully aromatic but nonconjugated linker. In BPTRZ, a meta-substituted biphenyl unit acts as connecting group whereas in MBPTRZ the biphenyl unit is additionally twisted by two methyl groups in 2- and 2'-position. BPTRZ and MBPTRZ are prepared using a triazine substituted with two carbazoles that we have described before.<sup>25</sup> The synthesis of the carbazole substituted unsymmetrical biphenyls **6** and **7** has been newly developed. Both materials represent versatile building blocks for the synthesis of unsymmetrically substituted matrix materials. The synthesis of the two host materials BPTRZ and MBPTRZ is outlined in Scheme 1. The electron deficient biscarbazolyl-triazine **1** is synthesized by a nucleophilic substitution of carbazole at the triazine core. The number of carbazole units is controlled by the ratio of carbazole and triazine and the reaction temperature. Due to the stepwise deactivation of the chlorines at the triazine core after substitution with an electron donating carbazole unit,<sup>25</sup> the reaction of two equivalents of carbazole with cyanuric chloride leads to **1** in 70% yield. The biphenyl building blocks for BPTRZ and MBPTRZ are synthesized by two different routes. For BPTRZ, 3,3'-dibromobiphenyl **2** is obtained by copper mediated homocoupling of 3-bromophenylboronic acid.<sup>28</sup> Via Goldberg-type reaction, one carbazole unit is attached to the biphenyl moiety to receive 3-(carbazol-9-yl)-3'-bromobiphenyl **4**.<sup>29</sup> The borylation of **4** is achieved by Miyaura-type cross coupling reaction.<sup>30</sup> Finally, BPTRZ is prepared by Suzuki-Miyaura cross-coupling reaction between the biscarbazolyl-triazine **1** and the borylated carbazole substituted biphenyl **6**.<sup>31</sup> MBPTRZ was prepared in a similar way except that 3,3'-diiodo-2,2'-dimethylbiphenyl **3** was

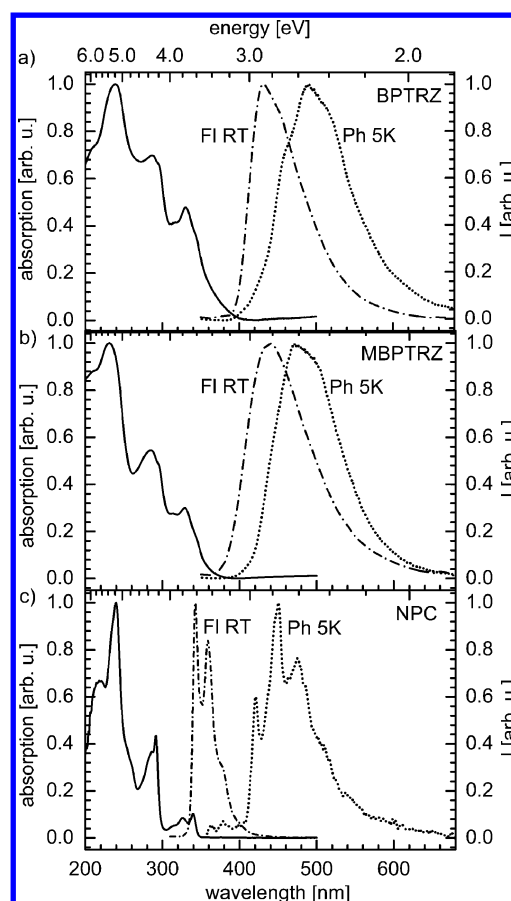


**Figure 2.** Absorption (solid line), fluorescence (dash-dotted line), and phosphorescence spectra (dotted line) of (a) BPTRZ, (b) MBPTRZ, and (c) N-phenylcarbazole (NPC) in neat film. Absorption and fluorescence (FI) were taken from thin films at room temperature, phosphorescence (Ph) (film) was taken at 5 K. In each subfigure, the bottom axis refers to wavelength and the top axis denotes energy.

used, which was synthesized by iodination of 2,2'-dimethylbiphenyl with iodine/iodic acid.<sup>11</sup> The following steps are analogous to BPTRZ, that is, Goldberg-coupling of carbazole, subsequent borylation, and Suzuki cross-coupling with **1** to MBPTRZ.

**Thermal Characterization.** The thermal properties of the triazines were investigated by differential scanning calorimetry (DSC), and their thermal stability was checked by thermogravi-

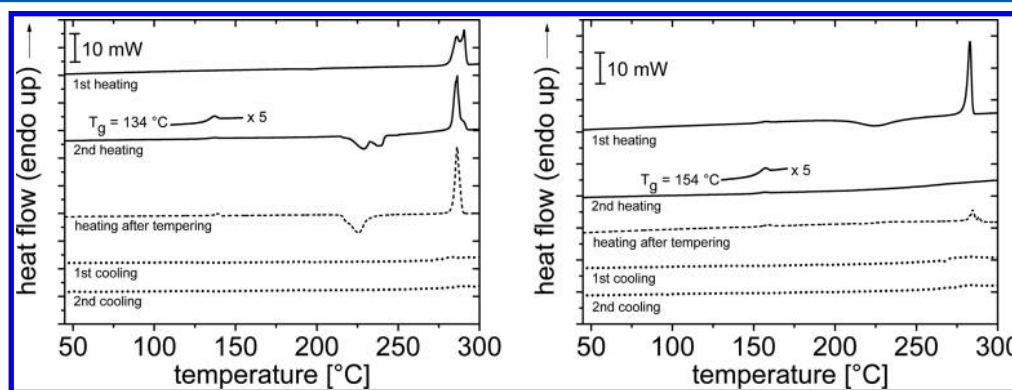


**Figure 1.** DSC-curves of BPTRZ (left) and MBPTRZ (right). Shown are the first and second heating scans, an additional heating scan after tempering the sample for 18 h at 100 °C as well as the first and second cooling scans at a scan speed of 10 K/min in  $N_2$ -atmosphere.

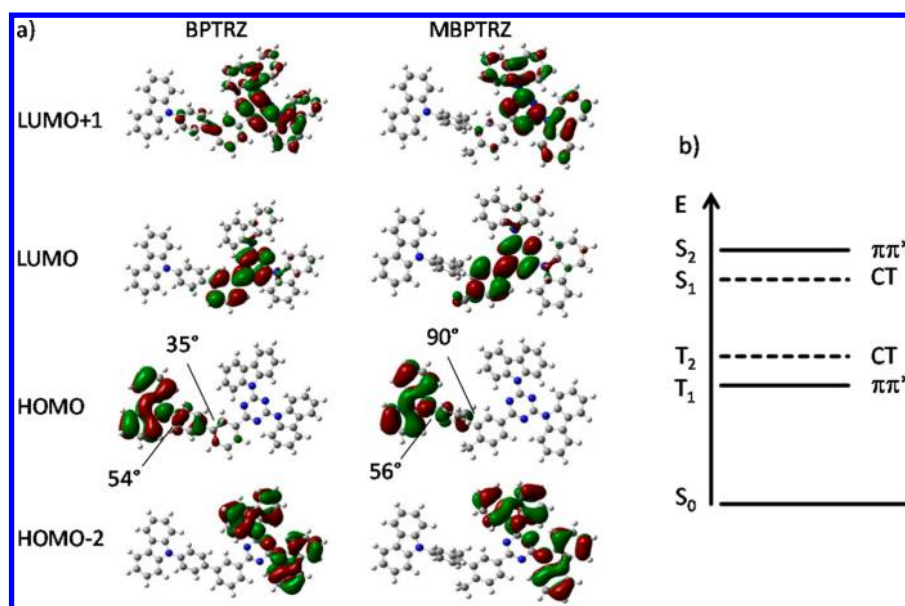


**Figure 3.** (a) DFT optimized ground state geometries for BPTRZ (left side) and MBPTRZ (right side), along with the orbitals having major contributions to the first and second singlet excited state. Also indicated are significant torsion angles between adjacent units. (b) Scheme indicating the order and dominant character of the first and second singlet and triplet excited states (see text).

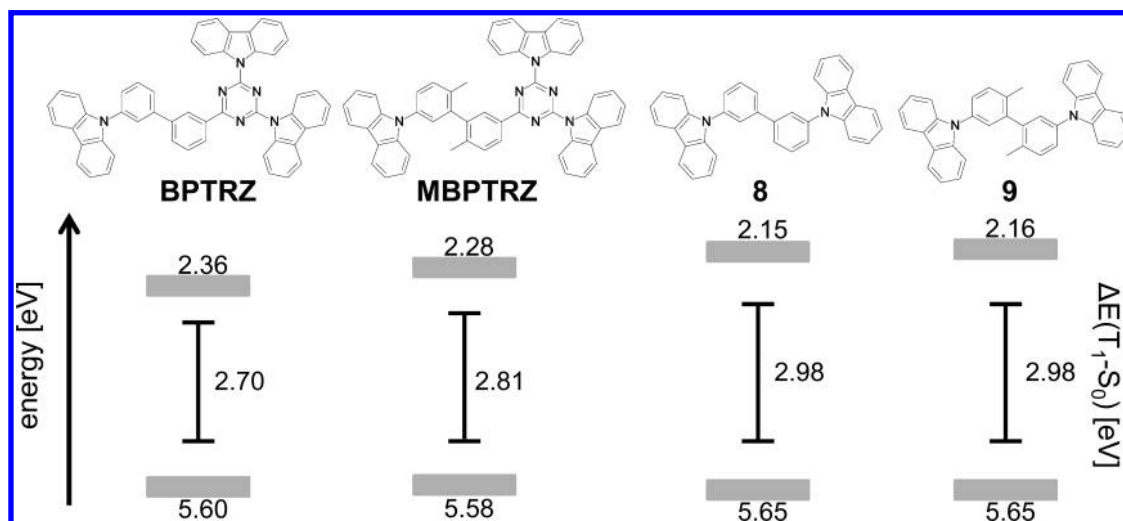


**Figure 4.** Energy diagram showing the location of the HOMO and LUMO levels of BPTRZ, MBPTRZ, and two CBP-derivatives 8 and 9 for comparison. The HOMO levels were determined from the half-wave potential of the first oxidation in the cyclic voltammetry experiment. The LUMO levels were estimated from the HOMO values and the optical bandgaps. The solid lines display the triplet energies  $\Delta E(T_1-S_0)$ .

**Table 2. Optical Properties of BPTRZ and MBPTRZ**

	$\lambda_{EA}^a$ [nm] film	$\Delta E(S_0-S_1)^b$ [eV]	$\lambda_{em}^{RTc}$ [nm] film	$\lambda_{em}^{SKd}$ [nm] film	$\Delta E(T_1-S_0)^e$ [eV]
BPTRZ	405	3.06	431	459	2.70
MBPTRZ	385	3.22	440	441	2.81

<sup>a</sup>Absorption edge measured in neat films at room temperature. <sup>b</sup>The optical bandgap was determined from the UV/vis absorption onset of neat films. <sup>c</sup>Fluorescence maxima (excitation: 330 nm,  $10^{-5}$  M cyclohexane solution, room temperature). <sup>d</sup>Wavelength of 0–0 phosphorescence transition measured on film samples (2 wt % matrix material in PMMA at 5 K). <sup>e</sup>The triplet energy was determined from the 0–0 transition of the phosphorescence spectra of neat films at 5 K.

metric analysis (TGA). In Table 1 the thermal data are summarized. TGA measurements show that both triazines BPTRZ and MBPTRZ possess high thermal stabilities of more

than 400 °C. A weight loss of 1% ( $T_d$ ) is observed at 445 °C for BPTRZ and 475 °C for MBPTRZ. These values are more than 100 °C above the sublimation temperatures of BPTRZ and MBPTRZ and therefore prove their high thermal stability. In Figure 1, the DSC curves are shown. BPTRZ exhibits a double melting peak at 286 and 290 °C. During cooling no phase transition can be seen. The  $T_g$  of BPTRZ is observed at 134 °C in the second DSC heating scan followed by two exothermic peaks at 228 and 236 °C corresponding to the recrystallization of the material. The melting of BPTRZ occurs again at 286 and 290 °C. To check the stability of the amorphous phase of BPTRZ formed during cooling we annealed the sample for 18 h at 100 °C. The heating curve shows a recrystallization at 226 °C and a melting at 286 °C.

MBPTRZ (Figure 1 right) exhibits a recrystallization peak in the range from 210 to 240 °C and an endothermic peak at 283

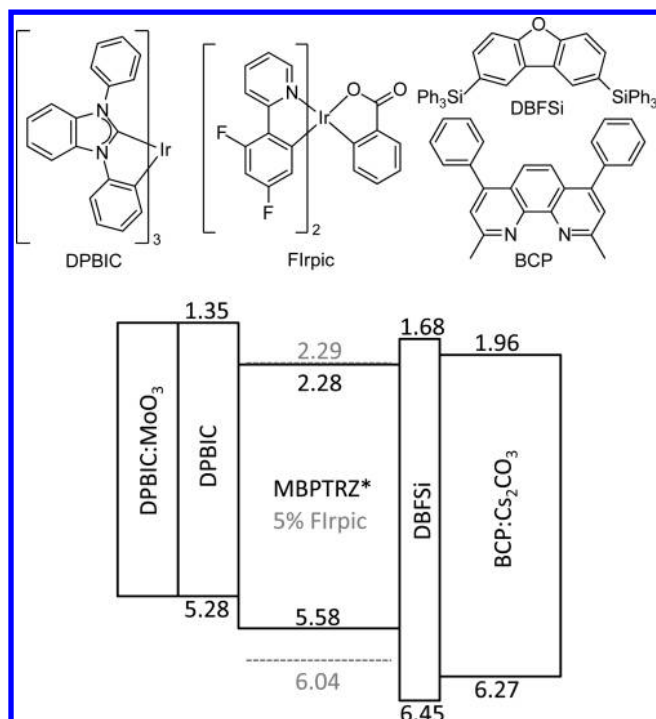


**Figure 5.** Top: Chemical structures of materials used in the OLEDs. Bottom: Energy level diagram of device 2 with MBPTRZ as host material; ionization potentials and electron affinity levels of the different materials are indicated. The dotted lines represent the levels of the emitter FIrpic. \* For device 1, BPTRZ with a HOMO level of 5.60 eV and a LUMO level of 2.36 eV was used as host material.

°C, which is assigned to the melting of the material and is only observed in the first heating. Upon cooling, the material solidifies in an amorphous state without recrystallization. Tempering MBPTRZ (18 h at 100 °C) leads to a small degree of

crystallization, which can be seen from the melting peak at 284 °C. The melting enthalpy is about 16% of the enthalpy during the first heating run, which demonstrates that only a small amount of the material has crystallized during tempering at 100 °C. The high recrystallization temperature in the range from 215 to 243 °C for BPTRZ and the small amount of recrystallization after tempering MBPTRZ at 100 °C demonstrate the stability of the glassy state in pure BPTRZ and MBPTRZ. In OLEDs the stability is usually further enhanced by mixing the matrix material with an emitter.

#### Spectroscopic Measurements and DFT Calculations.

The thin film absorption and emission spectra for BPTRZ and MBPTRZ are shown in Figure 2, along with the corresponding data for N-phenylcarbazole (NPC) for ease of comparison. The absorption spectra of BPTRZ and MBPTRZ are nearly identical. With increasing photon energy, they feature three bands of increasing oscillator strengths as well as a tail from about 3.44–3.10 eV (360–400 nm). This tail is also present in solution of BPTRZ and MBPTRZ, in contrast to the reference compound NPC. The lowest energy band shows a shoulder at 3.60 eV (344 nm) and peaks at 3.76 and 3.92 eV (329 nm, 316 nm). These features have an equidistant spacing of 160 meV (about 1290  $\text{cm}^{-1}$ ), which is a typical mean vibrational energy.<sup>32</sup> Furthermore, the peaks coincide with the energies of the 0–0, 0–1 and 0–2 vibrational peak of the first absorption band in NPC. Similarly, the second absorption band displays features at 4.19, 4.34, and 4.49 eV that concur with the vibrational peaks in the second absorption band of NPC. Evidently, the excited states in BPTRZ and MBPTRZ have significant contributions from transitions that are localized on the carbazole moieties.

The emission spectra were taken from thin films in two different ways such as to distinguish the short-lived intense fluorescence from the weak long-lived phosphorescence. To measure the fluorescence, we used a JASCO luminescence spectrometer at room temperature and excited at 3.75 eV (330 nm). In order to detect phosphorescence, the samples were

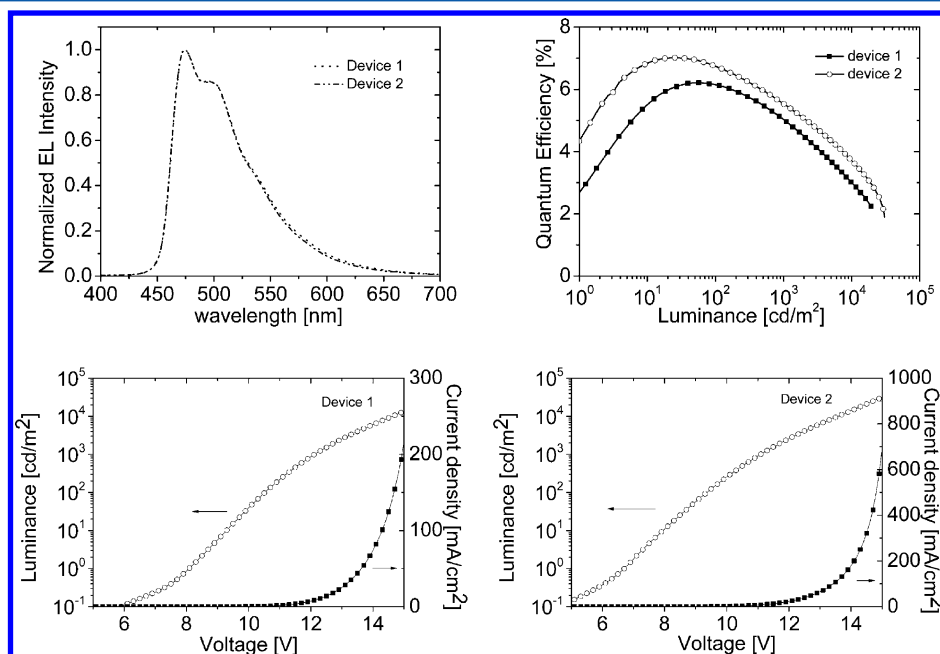


**Figure 6.** Top left: Electroluminescence spectra of the devices 1 (BPTRZ) and 2 (MBPTRZ). Top right: Quantum efficiency–luminance characteristics for the blue phosphorescent OLEDs with BPTRZ (device 1) and MBPTRZ (device 2) as host materials. Bottom: Luminance–voltage–current density characteristics for the blue phosphorescent OLEDs with BPTRZ (left) and MBPTRZ (right) as host materials.

Table 3. Performance of OLEDs using BPTRZ and MBPTRZ as Host Material for the Blue Emitter Flrpic<sup>a</sup>

	at 100 cd/m <sup>2</sup>				at 1000 cd/m <sup>2</sup>			
	voltage [V]	$\eta_C$ [cd/A]	$\eta_P$ [lm/W]	$\eta_{ext}$ [%]	voltage [V]	$\eta_C$ [cd/A]	$\eta_P$ [lm/W]	$\eta_{ext}$ [%]
BPTRZ	10.5	14.4	4.3	6.1	12.1	11.8	3.1	5.0
MBPTRZ	9.4	15.6	5.3	6.7	11.1	12.9	3.7	5.5

<sup>a</sup> $\eta_C$ : current efficiency;  $\eta_P$ : power efficiency;  $\eta_{ext}$ : external quantum efficiency.

cooled to 5 K, excited with a laser pulse at 3.68 eV (337 nm) and measured using a ICCD camera with gated detection. After a delay of 1  $\mu$ s with respect to the excitation pulse the gate was opened for 10 ms. The phosphorescence spectra for BPTRZ show peaks spaced about 160 meV apart at 2.70, 2.54, and 2.39 eV, with relative intensities that resemble the vibrational peaks in the NPC phosphorescence spectrum. MBPTRZ has essentially the same phosphorescence spectrum than BPTRZ, albeit shifted to higher energies by 110 meV and less structured. With these vibrational spacings and relative intensities, the phosphorescence spectra of MBPTRZ and BPTRZ look like the phosphorescence spectrum of N-phenylcarbazole, albeit somewhat broadened and shifted to the red by 140 meV for MBPTRZ and 250 meV for BPTRZ. In contrast to this resemblance in the phosphorescence spectra, the fluorescence of NPC and BPTRZ or MBPTRZ show marked differences. For the reference N-phenylcarbazole, the fluorescence is well-structured with narrow vibrational peaks and, in particular, without any noticeable Stokes' shift between the 0–0 peaks of fluorescence and absorption. In contrast to this, the fluorescence spectra of MBPTRZ and BPTRZ are broader and display a pronounced energy shift between the maximum of the fluorescence spectra and either shoulder or peak in the first absorption bands. Furthermore, the energy difference between the fluorescence spectra of NPC and MBPTRZ or BPTRZ is much larger than that found for the phosphorescence spectra.

In order to interpret these spectra, it is helpful to consider DFT calculations of the ground state geometry and the excited states, calculated using Gaussian with the B3LYP hybrid functional. In both compounds, BPTRZ and MBPTRZ, the central triazine ring forms an approximately planar system with the two adjacent carbazole moieties and the adjacent phenyl ring (Figure 3). The torsion angles between the triazine ring and the adjacent carbazoles is about 20°, and that with the adjacent phenyl ring is 15° for BPTRZ and 11° for MBPTRZ. This roughly planar half of the molecule is separated from the third carbazole unit by strong torsions, as indicated in the figure. Consistent with these strong torsions is a strong localization of the frontier orbitals. While the HOMO is localized onto the carbazole moiety, the LUMO is confined to the central triazine and the adjacent phenyl ring. Since hole transport takes place between HOMOs and electron transport between LUMOs, this implies that the transport pathways for both carriers are spatially separated even when they happen to meet on one molecule. We shall now consider the dominant transitions of the excited states. The first calculated excited state,  $S_1$ , involves mainly the transition from the carbazole-based HOMO to a triazine-based LUMO. In agreement with the strong charge-transfer (CT) character of this state, it carries no oscillator strength. The next higher excited state,  $S_2$ , is calculated to be 0.25 eV above  $S_1$  and has oscillator strength (0.08). The dominant transition occurs from the HOMO-2 to the LUMO+1. It has a strong  $\pi\pi^*$  character involving the  $\pi$ -system that extends over two carbazoles connected by the central triazine ring.

We associate the CT-type  $S_1$  state with the weak tail observed in the absorption spectra. We further consider that the broad and

red-shifted fluorescence results from this  $S_1$  state after geometric relaxation in the excited state and thus concomitant planarization and somewhat improved wave function overlap. By virtue of their small wave function overlap, charge transfer states are characterized by a small exchange energy, so that the associated triplet excited state can be expected to be energetically close. In contrast, the exchange energy associated with  $\pi\pi^*$  transitions is significantly larger, typically in the range 0.7–1.0 eV.<sup>33</sup> We therefore attribute the phosphorescence of BPTRZ and MBPTRZ to a triplet state based on  $\pi\pi^*$  transitions such as the HOMO-2 to LUMO+1 transition involved in  $S_2$ . Such an involvement of carbazole-based transitions between a  $\pi$ -systems extending over two connected carbazoles is in good agreement with the observed vibrational structure of the phosphorescence spectrum. A qualitative scheme of the excited state order is indicated in Figure 3. A similar relative order of states has also been observed for related carbazole-derivatives with charge transfer character.<sup>34</sup>

**Electrochemical Properties.** The electrochemical behavior was studied by cyclic voltammetry (CV). The HOMO levels were determined from the half-wave potential of the first oxidation relative to ferrocene and the LUMO levels were calculated by adding the optical band gap to the HOMO levels. The first oxidation events of BPTRZ and MBPTRZ are observed at 0.80 and 0.78 V (vs Fc/Fc<sup>+</sup>). The potentials can be translated to HOMO levels of 5.60 and 5.58 eV. In Figure 4, the HOMO and LUMO values of BPTRZ and MBPTRZ are compared to CBP-derivatives **8** and **9** from a previous paper.<sup>24</sup> In these materials, the meta-substituted biphenyl linkers are identical to BPTRZ and MBPTRZ, but the biphenyl units are substituted with carbazoles on both sides. The HOMO levels of all four matrix materials are between 5.58 and 5.65 eV and almost identical. The well-known host material CBP also has a HOMO of 5.63 eV. This shows that the HOMOs of all four materials are mainly located at the electron rich carbazole adjacent to the biphenyl linkers (Figure 3). The LUMOs of the triazine containing BPTRZ and MBPTRZ are at 2.36 and 2.28 eV, and therewith somewhat lower compared to the carbazole based compounds **8** and **9**. The triplet energies of **8** and **9** are both at 2.98 eV. In BPTRZ, where the meta-substituted biphenyl is linked to an electron withdrawing triazine unit, the triplet energy is at 2.70 eV. In MBPTRZ, where the two phenyl rings in the biphenyl unit are twisted by 90°, the triplet energy goes up to 2.81 eV (Table 2). This shows that an efficient decoupling of the electron donating and the electron accepting unit in bipolar host materials is important to achieve a high triplet energy. The triplet energy of 2.81 eV for MBPTRZ is high enough for blue emitters.

**Phosphorescent Organic Light-Emitting Diode.** To demonstrate the potential of BPTRZ and MBPTRZ as host materials for blue phosphorescent emitters, OLEDs were fabricated. The materials and the device setup are presented in Figure 5. On top of an indium–tin–oxide (ITO) glass substrate poly(3,4-ethylenedioxythiophene):poly(styrenesulfonate) (PEDOT:PSS) was spin coated as hole injection layer followed by 10 nm DPBIC p-doped with molybdenum(VI) oxide as hole

transporting layer. An additional 10 nm thick layer of tris[(3-phenyl-1H-benzimidazol-1-yl-2(3H)-ylidene)-1,2-phenylene]-iridium (DPBIC) followed as exciton and electron blocking layer. The 40 nm thick emission layer consisted of 5% Flrpic doped into the triazine host materials BPTRZ (device 1) or MBPTRZ (device 2). As hole and exciton blocking layer 5 nm of 2,8-bis(triphenylsilyl)-dibenzofuran (DBFSi) were deposited followed by 20 nm cesium carbonate doped 2,9-dimethyl-4,7-diphenyl-1,10-phenanthroline (BCP) as electron transporting layer. The devices were finalized by deposition of 100 nm aluminum as cathode.

Figure 6 (top left) displays the electroluminescence spectra of both devices at a current density of 5 mA/cm<sup>2</sup>. The two spectra are almost identical. Both devices show the pure emission of Flrpic with a maximum at 473 nm.

The luminance–voltage–current density characteristics and the efficiencies of the OLED devices 1 and 2 are shown in Figure 6 and summarized in Table 3. For OLEDs with BPTRZ as host 100 cd/m<sup>2</sup> are reached at 10.5 V and 1000 cd/m<sup>2</sup> at 12.1 V. For MBPTRZ, the corresponding voltages are lower at 9.4 V (100 cd/m<sup>2</sup>) and 11.1 V (1000 cd/m<sup>2</sup>). The maximum brightness is 24400 cd/m<sup>2</sup> (at 15.7 V) for BPTRZ and 30600 cd/m<sup>2</sup> (at 15.0 V) for MBPTRZ. Device 1 with BPTRZ as host material exhibit a maximum external quantum efficiency of 6.2% and a power efficiency of 4.6 lm/W, whereas device 2 with MBPTRZ reaches 7.0% and 6.3 lm/W, respectively.

## CONCLUSION

We have synthesized two new bipolar host materials BPTRZ and MBPTRZ with a hole transporting carbazole moiety that is separated from the electron transporting biscarbazolyl-triazine by a nonconjugated meta-linked biphenyl unit. Both host materials possess high thermal stabilities and good glass forming properties. The additional twist at the biphenyl unit in MBPTRZ, which is achieved by two additional methyl groups in the 2- and 2'-position of the biphenyl reduces the conjugation in MBPTRZ, leading to higher triplet energy of 2.81 eV compared to 2.70 eV for BPTRZ. A phosphorescent OLED with MBPTRZ as host and Flrpic as blue emitter has an external quantum efficiency of 7.0%, a current efficiency of 16.3 cd/A and a power efficiency of 6.3 lm/W. These results demonstrate the potential of donor-substituted triazines as bipolar host materials for blue phosphorescent OLEDs.

## AUTHOR INFORMATION

### Corresponding Author

\*E-mail: peter.strohriegl@uni-bayreuth.de.

### Notes

The authors declare no competing financial interest.

## ACKNOWLEDGMENTS

We thank I. Bauer for the help with the synthesis of the host materials and C. Lennartz, S. Watanabe, P. Schrögel, and M. Rothmann for helpful discussions. We are grateful to the Graduiertenkolleg GRK 1640 (German Science Foundation) and the BMBF (TOPAS 2012) for financial support.

## REFERENCES

- (1) Baldo, M. A.; O'Brien, D. F.; You, Y.; Shoustikov, A.; Sibley, S.; Thompson, M. E.; Forrest, S. R. *Nature* **1998**, *395*, 151.
- (2) Baldo, M. A.; Thompson, M. E.; Forrest, S. R. *Nature* **2000**, *403*, 750.
- (3) Adachi, C.; Kwong, R. C.; Djurovich, P.; Adamovich, V.; Baldo, M. A.; Thompson, M. E.; Forrest, S. R. *Appl. Phys. Lett.* **2001**, *79*, 2082.
- (4) Holmes, R. J.; Forrest, S. R.; Tung, Y.-J.; Kwong, R. C.; Brown, J. J.; Garon, S.; Thompson, M. E. *Appl. Phys. Lett.* **2003**, *82*, 2422.
- (5) Ren, X.; Li, J.; Holmes, R. J.; Djurovich, P. I.; Forrest, S. R.; Thompson, M. E. *Chem. Mater.* **2004**, *16*, 4743.
- (6) Sasabe, H.; Takamatsu, J.-i.; Motoyama, T.; Watanabe, S.; Wagenblast, G.; Langer, N.; Molt, O.; Fuchs, E.; Lennartz, C.; Kido, J. *Adv. Mater.* **2010**, *22*, 5003.
- (7) Adamovich, V.; Brooks, J.; Tamayo, A.; Alexander, A. M.; Djurovich, P. I.; D'Andrade, B. W.; Adachi, C.; Forrest, S. R.; Thompson, M. E. *New J. Chem.* **2002**, *26*, 1171.
- (8) Tanaka, I.; Tabata, Y.; Tokito, S. *Chem. Phys. Lett.* **2004**, *400*, 86.
- (9) Tokito, S.; Iijima, T.; Suzuri, Y.; Kita, H.; Tsuzuki, T.; Sato, F. *Appl. Phys. Lett.* **2003**, *83*, 569.
- (10) Gong, S.; He, X.; Chen, Y.; Jiang, Z.; Zhong, C.; Ma, D.; Qin, J.; Yang, C. *J. Mater. Chem.* **2012**, *22*, 2894.
- (11) Schrögel, P.; Langer, N.; Schildknecht, C.; Wagenblast, G.; Lennartz, C.; Strohriegel, P. *Org. Electron.* **2011**, *12*, 2047.
- (12) Duan, L.; Qiao, J.; Sun, Y.; Qiu, Y. *Adv. Mater.* **2011**, *23*, 1137.
- (13) Tsai, M.-H.; Lin, H.-W.; Su, H.-C.; Ke, T.-H.; Wu, C.-c.; Fang, F.-C.; Liao, Y.-L.; Wong, K.-T.; Wu, C.-I. *Adv. Mater.* **2006**, *18*, 1216.
- (14) Li, J.; Di Liu, Li, Y.; Lee, C.-S.; Kwong, H.-L.; Lee, S. *Chem. Mater.* **2005**, *17*, 1208.
- (15) Inomata, H.; Goushi, K.; Masuko, T.; Konno, T.; Imai, T.; Sasabe, H.; Brown, J. J.; Adachi, C. *Chem. Mater.* **2004**, *16*, 1285.
- (16) Chiu, T.-L.; Lee, P.-Y.; Lee, J.-H.; Hsiao, C.-H.; Leung, M.-K.; Lee, C.-C.; Chen, C.-Y.; Yang, C.-C. *J. Appl. Phys.* **2011**, *109*, 84520.
- (17) Su, S.-J.; Sasabe, H.; Takeda, T.; Kido, J. *Chem. Mater.* **2008**, *20*, 1691.
- (18) Chou, H.-H.; Cheng, C.-H. *Adv. Mater.* **2010**, *22*, 2468.
- (19) Chaskar, A.; Chen, H.-F.; Wong, K.-T. *Adv. Mater.* **2011**, *23*, 3876.
- (20) Liu, X.-K.; Zheng, C.-J.; Xiao, J.; Ye, J.; Liu, C.-L.; Wang, S.-D.; Zhao, W.-M.; Zhang, X.-H. *Phys. Chem. Chem. Phys.* **2012**, *14*, 14255.
- (21) Wang, Q.; Wallace, J. U.; Lee, T. Y.-H.; Ou, J. J.; Tsai, Y.-T.; Huang, Y.-H.; Wu, C.-C.; Rothberg, L. J.; Chen, S. H. *J. Mater. Chem. C* **2013**, *1*, 2224.
- (22) Chang, C.-H.; Kuo, M.-C.; Lin, W.-C.; Chen, Y.-T.; Wong, K.-T.; Chou, S.-H.; Mondal, E.; Kwong, R. C.; Xia, S.; Nakagawa, T.; Adachi, C. *J. Mater. Chem.* **2012**, *22*, 3832.
- (23) Rothmann, M. M.; Fuchs, E.; Schildknecht, C.; Langer, N.; Lennartz, C.; Münster, I.; Strohriegel, P. *Org. Electron.* **2011**, *12*, 1192.
- (24) Schrögel, P.; Tomkeviciene, A.; Strohriegel, P.; Hoffmann, S. T.; Köhler, A.; Lennartz, C. *J. Mater. Chem.* **2011**, *21*, 2266.
- (25) Rothmann, M. M.; Haneder, S.; Da Como, E.; Lennartz, C.; Schildknecht, C.; Strohriegel, P. *Chem. Mater.* **2010**, *22*, 2403.
- (26) Becke, A. D. *J. Chem. Phys.* **1993**, *98*, 5648.
- (27) Lee, C.; Yang, W.; Parr, R. G. *Phys. Rev. B* **1988**, *37*, 785.
- (28) Cheng, G.; Luo, M. *Eur. J. Org. Chem.* **2011**, *2011*, 2519.
- (29) Klapars, A.; Antilla, J. C.; Huang, X.; Buchwald, S. L. *J. Am. Chem. Soc.* **2001**, *123*, 7727.
- (30) Ishiyama, T.; Murata, M.; Miyaura, N. *J. Org. Chem.* **1995**, *60*, 7508.
- (31) Su, S.-J.; Cai, C.; Kido, J. *Chem. Mater.* **2011**, *23*, 274.
- (32) Köhler, A.; Khan, A. L. T.; Wilson, J. S.; Dosche, C.; Al-Suti, M. K.; Shah, H. H.; Khan, M. S. *J. Chem. Phys.* **2012**, *136*, 94905.
- (33) Köhler, A.; Wilson, J. S.; Friend, R. H.; Al-Suti, M. K.; Khan, M. S.; Gerhard, A.; Bässler, H. *J. Chem. Phys.* **2002**, *116*, 9457.
- (34) Hoffmann, S. T.; Schrögel, P.; Rothmann, M.; Albuquerque, R. Q.; Strohriegel, P.; Köhler, A. *J. Phys. Chem. B* **2010**, *115*, 414.